Environmental Science Nano

Impacts of Particle Surface Heterogeneity on the Deposition of Colloids on Flat Surfaces

Journal:	*Environmental Science: Nano*
Manuscript ID	EN-ART-01-2021-000049.R3
Article Type:	Paper

Environmental Significant Statement

In the natural environment, the surfaces of particles are always heterogeneously charged and may partially be covered with natural organic matter or other functional groups. The surface heterogeneity properties can play a more important role in deposition than the overall surface potential of particles. We have shown that deposition did not occur even though the overall zeta potential of Janus SiO_2 NPs was opposite that of the deposition surface due to the dominant role of surface heterogeneity created by PLL. PLL has been used in many previous studies to simulate positively charged surfaces in the environment. The results of this study will provide guidance on modeling the transport and deposition of nanoparticles with heterogeneously charged surfaces in environmental settings.

Impacts of Particle Surface Heterogeneity on the Deposition of Colloids on Flat Surfaces

Thompson Delon[1], Tanushree Parsai[4], Ufuk Kilic[2], Mathias Schubert[2], Stephen A. Morin[3], and Yusong Li[1*]

[1]Department of Civil and Environmental Engineering, University of Nebraska-Lincoln, Lincoln, NE 68588

[2] Department of Electrical and Computer Engineering, University of Nebraska-Lincoln, Lincoln, NE 68588

[3]Department of Chemistry, University of Nebraska-Lincoln, Lincoln, NE, 68588

[4]Department of Civil Engineering, Indian Institute of Technology Delhi, 110016, India

[*]Corresponding author. Tel.: (402)-472-5972; fax: (402)-472-8934; Email: yli7@unl.edu

Abstract

Natural particles possess varying degrees of surface heterogeneities. Although the impact of collector surface heterogeneity on particle deposition is more or less established, the impact of particle surface heterogeneity on the deposition of colloids in porous media is not well studied. In this work, Janus SiO_2 microparticles (Janus SiO_2 MPs) were engineered by partially covering SiO_2 microspheres (500 nm in diameter) with positively charged poly(L-lysine) (PLL) as model particles to study the impact of particle surface heterogeneity on the deposition. The surface heterogeneity of Janus SiO_2 MP was confirmed using Kelvin probe force microscopy. Up to 4-5 original SiO_2 microspheres tended to assemble in the solution to form relatively stable clusters, with an isoelectric point slightly higher than pH 7. Compared with unmodified SiO_2 microspheres, Janus SiO_2 MPs had a slower attachment rate on silicon dioxide surfaces. While the deposition of Janus SiO_2 MPs onto silicon dioxide surfaces was observed at pH values of 3 and 7, no deposition was observed at pH 9. No deposition was observed for Janus SiO_2 MPs onto aluminum oxide surfaces for pH values ranging from 3 to 9, even under an overall favorable attractive condition. This work found that the deposition of colloids is more sensitive to particle surface heterogeneity properties than to the overall surface potential of the colloids.

Keywords: Surface Heterogeneity; Janus Particles; Transport; Deposition.

1. Introduction

Understanding the transport and deposition of colloids in porous media is very important to protect water resources. Colloid filtration theory (CFT) has been widely used to model colloid transport, by including three approaching mechanisms, including diffusion, interception, and sedimentation.[1] When particles approached the vicinity of the porous media surface (or the collector surface), the interaction energies, including attractive van der Waal (vdW), electric-double layer (EDL), and other additional energies (e.g., Born, Lewis acid-base, and steric interaction), between particles and collector surfaces control the colloid attachment step. The primary challenge in predicting colloid attachment arose from conditions when the approaching particle and the collector surface were likely charged, or under an unfavorable condition.[2] Although the theory predicts no attachment in the presence of an energy barrier created by the EDL repulsion under unfavorable conditions, numerous experimental fact that contradict theoretical expectations.[3] The discrepancy was attributed to the theoretical calculations based on measured bulk surface parameters.[4] Recent work has demonstrated that the inclusion of discrete representative nanoscale heterogeneity induced by heterodomains on the collector surfaces can largely reduce the gap between prediction and observations under favorable conditions.[4,5]

While attentions were given to the surface heterogeneity of collector surfaces, colloidal particles are still mainly considered as spherical and homogeneous. Natural colloids of biological and nonbiological origin, however, are anisotropic in nature, possessing varying degrees of surface heterogeneity. [6-14] Heterogeneous surfaces consist of microscopic domains with different characteristics, such as different chemical functionalities, hydrophobic/hydrophilic properties, and surface charges. For example, the step-like surface potential distribution on clay particle layers, which is due to heterogeneous charge, has been directly revealed by Kelvin probe force

microscopy (KPFM) and electrostatic force microscopy (EFM). [15] The cell surfaces of the Fe(III)-reducing bacteria *Shewanella putrefaciens* were found to contain electrochemically heterogeneous sites, resulting in a significant charge contrast. [16]

Very few studies have investigated the role of particle surface heterogeneity on their deposition. Colloid surface charges are often described based on their mean-field (or averaged) surface properties, e.g., the measured zeta potentials. Such an averaged approach can be misleading. As demonstrated by Drelich and Wang, [9] even if the measured net surface potential of several types of particles is similar, the particles are very differently charged, i.e., different heterogeneous patch sizes and distributions exist over the particle surface. Wang and Keller [8] demonstrated that for natural soil or clay colloids, the measured zeta potentials cannot be used as an indicator for predicting their transport and retention behavior in porous media due to the heterogeneous nature of these colloids. A recent study [17] investigated the attachment of microspheres with nanoscale heterogeneity created by randomly distributed poly(L-lysine) (PLL) in a shear flow. It was found that the attachment rate of particles onto chamber walls is largely dependent on the probability of the PLL group interaction with the chamber wall during particle transport. Additionally, deposition was found to be more sensitive to the heterogeneity of the particle surface than to the heterogeneity of the surface of chamber walls. In another modeling study [18], particle surface charge heterogeneity was incorporated into a 3-D trajectory model to simulate rod-shaped particle translation and rotation. The modeling results indicated that the location of particle surface heterogeneity predominantly affected colloid-surface interactions by influencing the possibility of heterogeneous patches facing the collector when particles rotate. By incorporating nanoscale heterogeneity on both colloid and collector surfaces, a very recent study was able to use particle trajectory modeling to predict the attachment of colloid particles in

impinging jet experiments.[19] While the crucial role of particle surface heterogeneity is being gradually identified, [17,18] a systematic understanding is still lacking. The initial impact of particle surface heterogeneity on the transport and retention of colloids can be even more complicated when considering the chemical composition of the background solution, properties of the collector surfaces, and flow conditions.

The objective of this study is to experimentally demonstrate the effects of colloid surface heterogeneity on particle deposition. We hypothesize that colloid surface heterogeneity, instead of the overall zeta potential, controls their deposition. We test this hypothesis by measuring the deposition of particles engineered with two distinctive surface properties, or Janus particles. Janus particles [19] are named after the Roman god "Janus", who has two faces looking in different opposite directions, and describe a special class of colloidal particles with a different chemical composition on their two hemispheres.[20-22] The Janus particles synthesized in this study were used as a model to represent particle surface heterogeneity condition of natural colloids.

2. Materials and Methods

2.1. Janus particle synthesis procedure

By modifying a previously published procedure,[23], we produced Janus particles by covering a portion of SiO_2 microsphere (500 nm in diameter) surfaces with PLL, a water-soluble polypeptide composed of naturally occurring L-lysine with a positively charged amine group on its side chain. Silicon (IV) Oxide microspheres in powder form with an average particle size of 500 nm (99.9%) and density of 2.0 g/cm^3 was purchased from Alfa Aesar (Massachusetts, USA). The surface of SiO_2 microspheres was cleaned with a piranha solution (a mixture of H_2SO_4 and H_2O_2) and rinsed with nanopure water (18.2 MΩ-cm, Barnstead Nanopure system). SiO_2 microspheres were dried at 80°C in an oven overnight and dispersed into a 1% wt/wt solution of

4:1 deionized (DI) water: ethanol in an ultrasonic water bath (FS 60, 100 W, 42 kHz, Fisher Scientific, Pittsburg, PA).

Si wafers were cut into a size of approximately 1 x 1 cm^2; cleaned by sonication with acetone, isopropyl alcohol (IPA) and DI water for 30 min, 20 min, and 10 min, respectively; and dried with N_2 gas. The surface was made hydrophilic by submerging the wafers in piranha solution for 12 hours, followed by rinsing with DI water and drying under N_2 gas. A superhydrophilic surface was achieved by submerging the wafers in a solution of DI water: NH_4OH: H2O2 at a ratio of 5:1:1 by volume at 80°C and then rinsing and drying. [24]

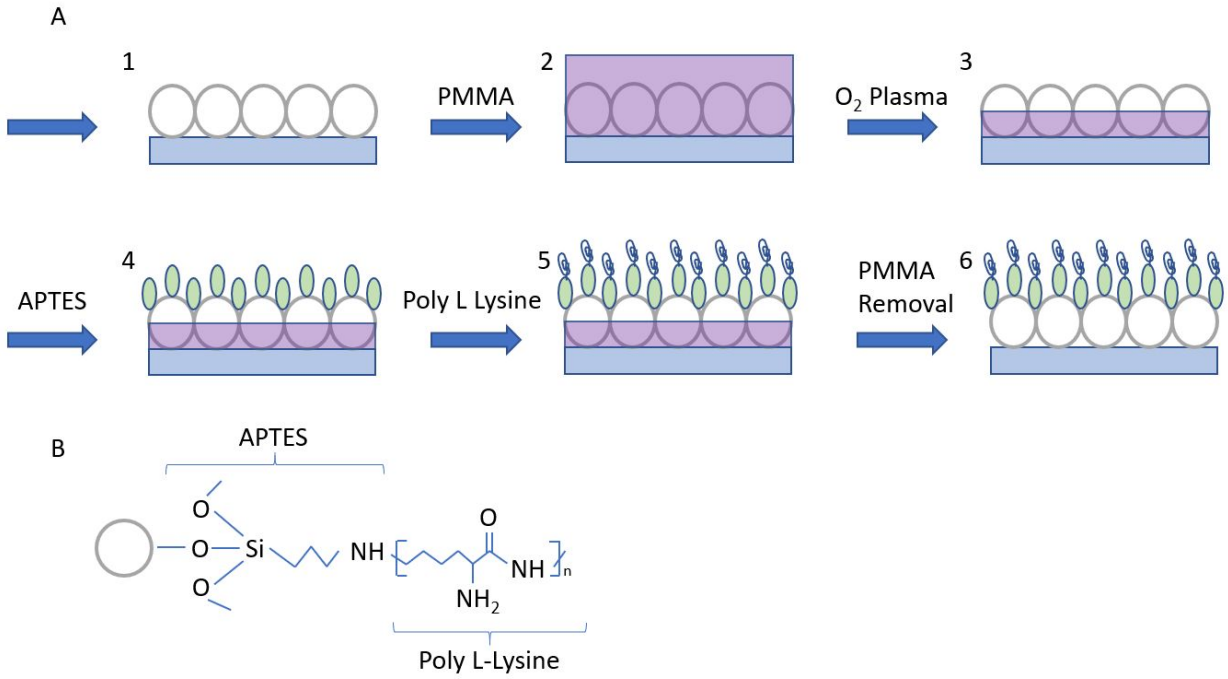

Figure 1. (A) Schematic diagram of Janus particle synthesis and (B) molecular structure of a single Janus particle. Green circles denote APTES, and blue curves denote PLL.

Two hundred microliters of SiO_2 microsphere solution was spin-coated on the surfaces of Si wafers at rates of 200 rpm, 1000 rpm, and 2000 rpm for 60 s, 120 s, and 15 s, respectively,

creating a single particle layer on the Si wafer, as illustrated in Figure 1. After drying, 90 μL of 10% w/v PMMA solution was spin-coated at 3000 rpm for 60 s (step 2). The wafer was left at room temperature for several hours to allow smooth uniform coverage of PMMA and then annealed for 2 hours at 90°C. The sample was then exposed to O_2 plasma to partially remove the PMMA layer from the sample (step 3). This process generated openings in the PMMA layer on top of the SiO_2 microspheres, which were available for further chemical modification. By controlling the duration of O_2 plasma exposure, we controlled the thickness of the removed PMMA layer and the size of the SiO_2 MP surfaces for further modification. Figure S1 (Supporting Information) shows SEM images of PMMA coverage on SiO_2MPs after exposure to O_2 plasma for different lengths of time. Based on our systematic optimization and error tests, it was determined that 1.75 min was needed to remove approximately half of the PMMA layer, and 20 min was needed for complete removal of the PMMA layer.

SiO_2 microspheres partially covered with PMMA were submerged in a mixture of 0.95 μL of APTES and 5 mL ethanol for 1 day on top of an orbital shaker, to functionalize the exposed portion of the SiO_2 microsphere surfaces with the NH_2 functional groups in APTES (step 4, Figure 1). Excess APTES was removed by rinsing with DI water and drying with N_2 gas. The sample was subsequently submerged in PLL solution for 1 hour to allow PLL to bond with the NH_2 functional groups in APTES, creating positively charged surfaces (step 5, Figure 1). Excess PLL was removed by rinsing with DI water and drying with N_2 gas. The PMMA coverage was then removed by shaking the Si wafer in acetone solution on an orbital shaker for 5 minutes, rinsing with DI water, and drying with N_2 gas. SiO_2 microspheres partially covered with PLL, namely, Janus SiO_2 microparticles (Janus SiO_2 MPs), were dispersed in 1 mM NaCl solution at pH 7 in an ultrasonic water bath (step 6, Figure 1).

For comparison, we synthesized control SiO_2 MPs and PLL-SiO_2 MPs. Control SiO_2 MPs refer to SiO_2 microspheres subject to all procedures and chemicals until step 3 of the Janus MP synthesis procedure (Figure 1), with subsequent complete PMMA removal by exposure to O_2 plasma for 20 min and acetone cleaning. Control SiO_2 MPs were exposed to all chemicals to which the Janus SiO_2 MPs were exposed to, except APTES and PLL. PLL-SiO_2 MPs were created with procedure to synthesize the control SiO_2 MPs and were then exposed to APTES and PLL to achieve full PLL coverage. The number-weighted hydrodynamic diameter distribution and zeta potential of all particles were measured using a 90Plus particle size analyzer and ZetaPals zeta potential analyzer, respectively (Brookhaven Instruments Corporation, Holtsville, NY).

2.2. Kelvin Probe Force Microscopy (KPFM) Imaging Procedure

Janus SiO_2 MPs dispersed in DI water were spin-coated on Si wafers. Each Si wafer was left to dry under ambient conditions before being placed onto an atomic force microscope (AFM) stage. KPFM images were obtained using a Bruker Dimension ICON AFM operating in the peak force KPFM mode. The interleave amplitude was 2 V, with a peak force amplitude and frequency of 150 nm and 2 kHz, respectively. A Bruker's new SCM-PIT-V2 platinum-iridium-coated tip (cantilever length 225 μm, resonance frequency 65 kHz, spring constant 2.8 N/m) and a D scan head (maximum scan area is 5 x 5 μm^2) were used. Scan rates were set to 0.498 Hz in tapping KPFM mode at a 100 nm lift scan height. The KPFM images were processed using Nanoscope analysis software.

2.3. Quartz Crystal Microbalance with Dissipation (QCM-D) experiments

QCM-D experiments were performed to evaluate the deposition of control SiO_2, Janus SiO_2, and PLL-SiO_2 MPs onto silicon dioxide- and aluminum oxide-coated QCM sensor

surfaces. In these experiments, water chemistry was maintained as 1 mM NaCl at pH 7. All three types of MP suspensions were determined to be relatively stable within 40 mins under this water chemistry. The detailed procedure of QCM-D experiments is provided in the supporting information.

3. Results and Discussion

3.1 KPFM surface charge distribution

KPFM is a scanning probe-based technique that allows investigation of the surface charge distribution.[25] Figure 2A shows the surface potential distribution of a single Janus SiO_2 MP on the surface of a Si wafer. The surface height of this Janus SiO_2 MP (Figure 2B), as shown along a cross section indicated by a white vertical line in Figure 2A, reached a maximum of 710 nm. As shown here, the surface potential on the Si wafer was approximately constant, while the surface potential on the Janus SiO_2 MP was heterogeneously distributed. A large part of the Janus SiO_2 MP was negatively charged, indicated by the green color. Part of the top surface was positively charged relative to the surface of the silica wafer, as indicated by the purple color. Figures 2B and provide a cross-sectional analysis of the Janus SiO_2 MP surface potential. In the vertical cross section (Figure 2C), the surface potential varied drastically. In the horizontal cross section (Figure 2B), the surface potential of the Janus SiO_2 MPs gradually increased from -0.5 mV to 3.07 V relevant to the silica wafer surface. Although the surface potential in the horizontal direction did not fluctuate as much in as the vertical direction, the graduate increase also represents surface heterogeneity. The positive charge on the surface suggests successful bonding of PLL, a positively charged polymer, on the surface of the Janus SiO_2 MP. The oscillation of the surface potential in the vertical cross section indicates that the surface coverage of PLL is not homogeneous. PLL was attached on top of APTES, which only bonded to favorable sites on the

surface of SiO_2 MPs. The heterogeneous surface potential distribution of the particles showed that the procedure described above led to synthesis of heterogeneously charged Janus SiO_2 MPs. Janus SiO_2 MPs synthesized following this approach were used as a model to represent the surface charge heterogeneity of natural colloids of biological and nonbiological origin.

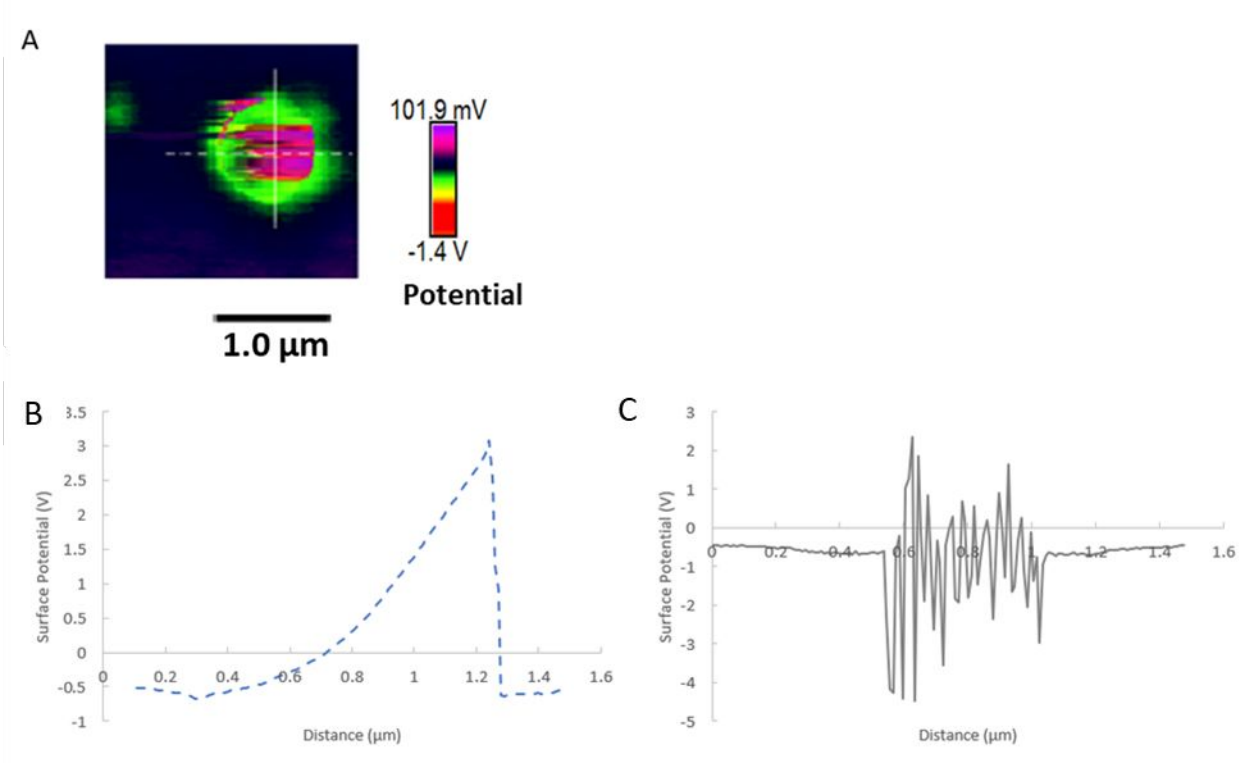

Figure 2. (A) Surface potential distribution map of a Janus SiO_2 MP on the surface of a Si wafer measured by KPFM; (B) surface potential distribution along the dashed horizontal white line (from left to right) in (A); (C) surface potential distribution along the vertical solid white line (from top to bottom) in (A).

3.2 Stability of particle size distribution.

The stability of the particle size distribution was investigated for control SiO_2 MP, Janus SiO_2 MP, and PLL-SiO_2 MP suspensions in 1 mM NaCl at pH at 0 min, 10 min, and 40 min after sonication (Figure 3). Figure 3A shows that the control SiO_2 MPs had an average particle diameter of 712.4 nm, ranging from 299.4 nm to 1433.9 nm. The distribution of control SiO_2

MPs was sharp and maintained almost no change within the first 10 min. The particle size distribution only slightly shifted to the right after 40 min, which showed that a small number of particles could form aggregates during this period.

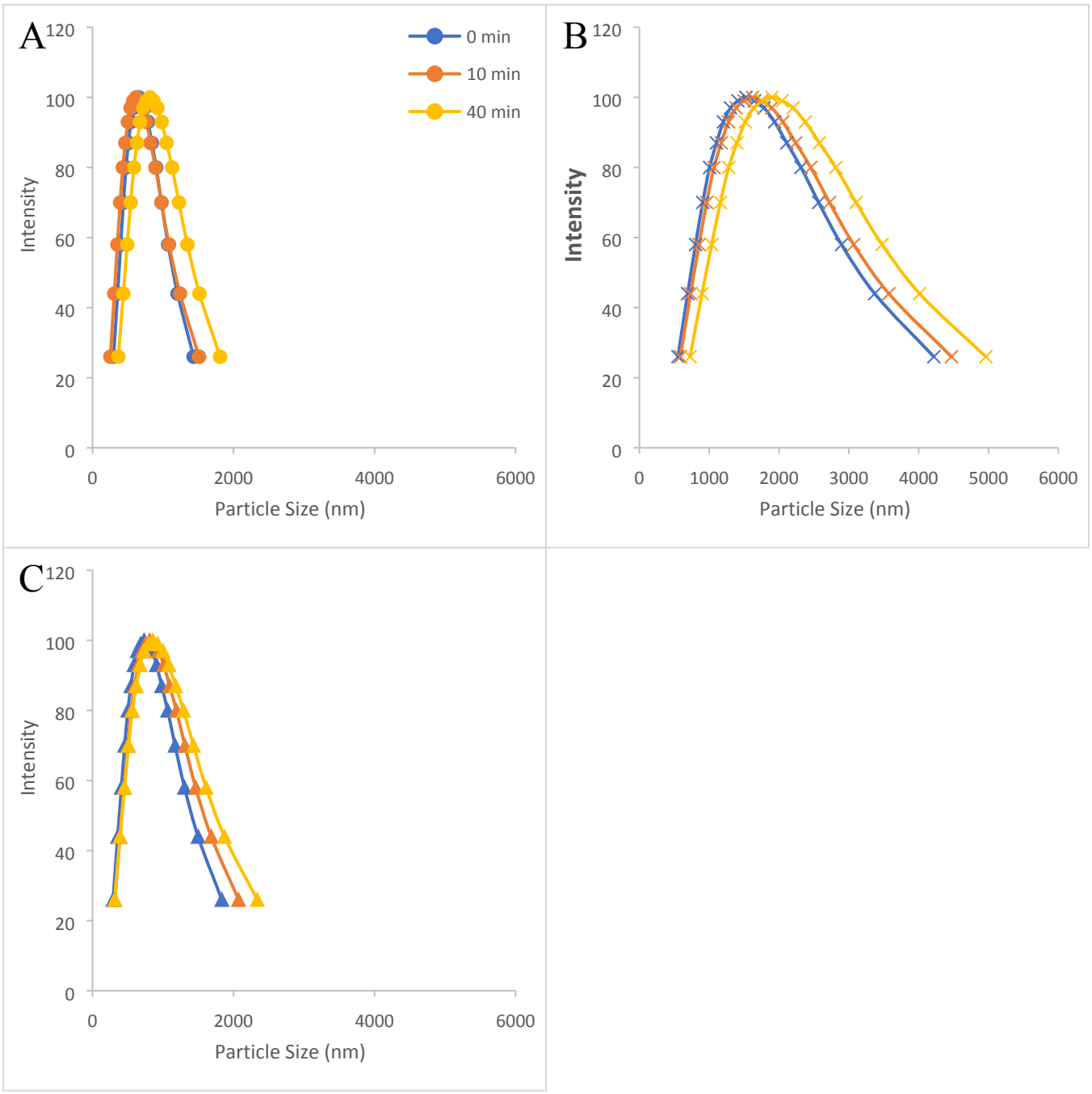

Figure 3. Particle size distribution of (A) control SiO_2 MPs, (B) Janus SiO_2 MPs, and (C) PLL-SiO_2 MPs in 1 mM NaCl pH 7 solution at different wait times: 0 min (blue), 10 min (orange), and 40 min (yellow) after the sonication process.

The mean particle diameter of PLL-SiO_2 MPs was 820.7 nm at 0 min, which was slightly higher than that of control SiO_2 MPs (Figure 3C). The slightly higher mean particle size of PLL-SiO_2 MPs could be attributed to the PLL layer adsorbed on the surface of positive SiO_2 MPs. According to a previous study,[26] the mean chain length of PLL was 207 nm at pH 7.5 in 5 mM bis-tris-propane buffer. The particle size distribution of PLL-SiO_2 MPs remained relatively stable, with a slight increase in larger sized particles over time. The particle size distribution of Janus SiO_2 MPs (Figure 3B) was wider than that of both control SiO_2 and PLL-SiO_2 MPs. At 0 min, the mean particle size of Janus SiO_2 MPs was 1755.6 nm and ranged from 552.4 nm to 4217.1 nm. The presence of much larger sizes of Janus SiO_2 MPs indicated aggregate formation in the Janus particle suspension. Janus particles were partially positively charged with PLL and partially negatively charged. Part of the particle surface of a Janus particle may attract the oppositely charged surfaces of other Janus particles.

Hong et al. [27] indicated that charged Janus particles may assemble to form equilibrated aggregates. Molecular simulations showed that half of each cluster was predominantly positively charged, while the other half was predominantly negatively charged. Thus, the charge asymmetry of individual Janus particles was preserved in the cluster, which probably was also the case in our Janus SiO_2 MP suspension, where up to 4-5 original SiO_2 MPs assembled in the solution to form primary heteroaggregates at the higher end of the particle size distribution. With increasing time, the distribution of Janus SiO_2 MPs became slightly wider and slightly shifted to larger value at 40 min, which indicated slightly increased aggregation over time. Theoretically, the positive side of one cluster will attract the negative side of another cluster over time, resulting in secondary aggregate formation. Because the concentration of Janus SiO_2 MPs in the

suspension was low (i.e., 10 ppm), the cluster formation was relatively slow. Because the particle size distribution did not show a significant change in the 40-minute period, the Janus SiO_2 MP suspensions can be considered relatively stable within this time framework.

3.3 Impact of Ionic Strength on the Zeta Potential of Janus MP Suspensions

We determined the zeta potentials of Janus SiO_2 MP suspensions in a range of IS and compared them with the zeta potentials of control SiO_2 MPs and PLL-SiO_2 MPs for freshly made solutions (Figure 4A) and solutions 20 minutes after sonication (Figure 4B). For freshly made MP solutions in 1 mM NaCl at pH 7, control SiO_2 MPs carried a negative charge of -37.7 mV, as expected.

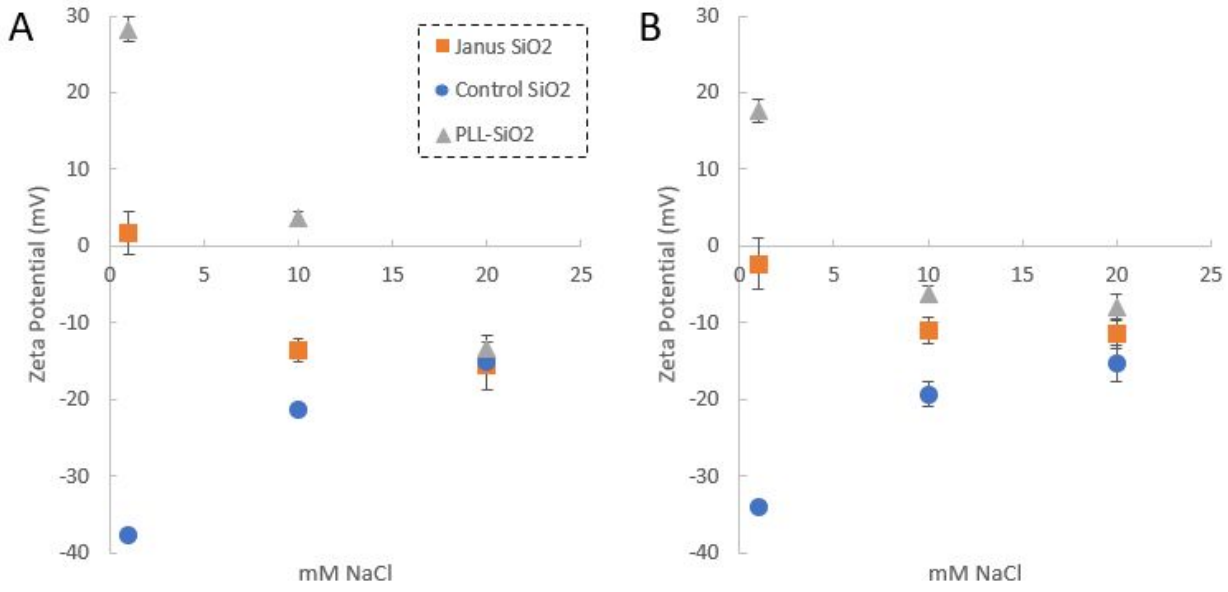

Figure 4. Zeta potential of control SiO_2 MPs, Janus SiO_2 MPs, and PLL-SiO_2 MPs at different ionic strengths in pH 7 solution at 0 min (A) and 20 min (B) after sonication.

The PLL-SiO_2 MPs had a positive charge of 28.3 mV in 1 mM NaCl, indicating that the surfaces of these particles were well covered by positively charged PLL. The zeta potential of

Janus SiO_2 MPs was 1.7 mV in 1 mM NaCl. The slightly positively charged zeta potential indicated that the surface of Janus SiO_2 MPs was half negative and other half predominantly positive, exhibiting surface conditions similar to those of the control SiO_2 MPs and PLL-SiO_2 MPs, respectively. Therefore, the overall surface potential, or zeta potential, was slightly positively charged.

With an increase in IS, the zeta potential values of the control SiO_2 MPs became less negative, as expected. For both PLL-SiO_2 MPs and Janus SiO_2 MPs, zeta potential values significantly decreased from positive to negative, with increasing IS. The decrease in zeta potential under higher IS for PLL-SiO_2 MPs and Janus SiO_2 MPs can be attributed to modification of the PLL conformation due to the change in cations in the solution. PLL is an interesting polypeptide material whose secondary structure can be converted to an α-helix, β-sheet, or random coil based on its surrounding water chemistry (e.g., solvents and temperatures).[26] While PLL is typically in a random coil conformation at a neutral pH, the presence of ionic species can change its conformation to an α-helix. In this work, with the increase in IS, PLL was converted from a random coil, a relatively loose structure, to an α-helix, a relatively compressed structure. We hypothesize that the flat α-helix conformation of PLL will allow more negatively charged sites on the surface of SiO_2 MPs to be exposed, leading to more negative zeta potential values. The reorganization has smaller effects on the zeta potential for Janus MPs compared with PLL-SiO_2 MPs due to the smaller amount of PLL attached to the Janus MP surface.

Twenty minutes after sonication (Figure 4B), the zeta potential values of the control SiO_2 MPs became slightly less negative, decreased from -37.7 mV and -21.3mV to -34 mV and -19.3 mV for 1 mM and 10 mM NaCl, respectively. At 20 mM NaCl, the zeta potential of control SiO_2 MPs remains constant. The zeta potential of PLL-SiO_2 MPs decreased from 28.3 mV at 0

minutes after sonication (Figure 4A) to 17.7 mV at 20 minutes after sonication (Figure 4B). Similarly, the zeta potential of Janus SiO_2 MPs was reduced from 1.7 mV (Figure 4A) at 0 minutes to -2.3 mV (Figure 4B) at 20 minutes after sonication. The reduction in zeta potential over time is consistent with the slight increase in particle size over time (Figure 3), both of which may be attributed to cluster formation over time. Twenty minutes after sonication, the zeta potential values of both Janus SiO_2 MPs and PLL-SiO_2 MPs showed the same decreasing trend with the increase in IS (Figure 4B) due to the conformational change of PLL under higher IS.

3.4 Impact of pH on the Zeta Potential of Janus MP suspensions

The zeta potentials of Janus SiO_2 MPs, PLL-SiO_2 MPs and control SiO_2 MPs in 1 mM NaCl are reported in Figure 5 when the pH was varied from 3 to 10. With the increase in pH value, more hydroxides were added to the suspension, and thus, the particles tended to acquire more negative charge. Previous work [28] has reported that SiO_2 particles have a negative zeta potential when the pH is higher than 2, which is consistent with our data. The zeta potential of the PLL-SiO_2 MPs decreased from 31.9 mV at pH 3 to -16.9 mV at pH 10. The isoelectric point, or the pH at which the particle zeta potential is zero, was between pH 7 and 9. The zeta potential of Janus SiO_2 MPs decreased from 7.6 mV at pH 3 to –23 mV at pH 10. The zeta potential of Janus SiO_2 MPs at pH 7 was 1.7 mV, indicating that the isoelectric pH point for Janus SiO_2 MPs is just slightly higher than 7. The change in the zeta potential of Janus SiO_2MPs was relatively flat under acidic conditions (pH <7), while a sharp drop occurred from 1.7 mV to -23 mV when the pH > 7.

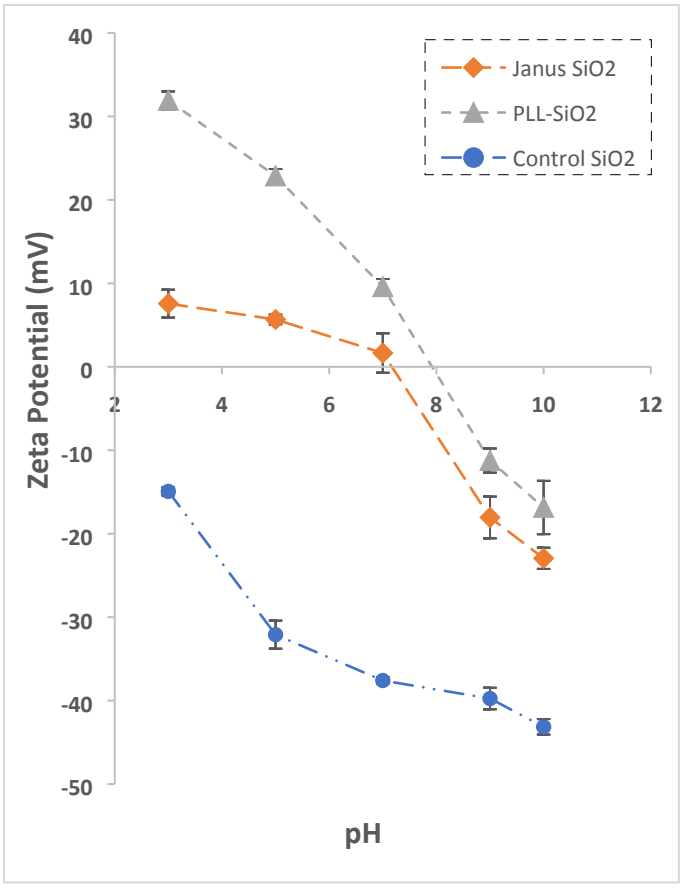

Figure 5. Impact of pH on the zeta potential of SiO_2MPs, Janus SiO_2 MPs, and PLL-SiO_2 MPs in 1 mM NaCl.

Previous work [28] has reported a strong effect of pH on the zeta potential of PLL. According to Naassaoui and Aschi, [29] the zeta potential of PLL remained relatively stable at approximately 40 mV when the pH was less than 5.2. With increasing pH, the zeta potential of PLL quickly decreased and approached neutral at a pH value of 10.6. Experimental results and molecular simulations also showed that the PLL conformation changed from random coil to α-helix with an increase in pH value. For Janus SiO_2 MPs and PLL-SiO_2 MPs, the zeta potential of PLL adsorbed on the SiO_2 surface decreased with the increase in pH, leading to reduced overall particle zeta potentials. In addition, with PLL conversion from random coil to α-helix, the

resulting more compact structure will expose negatively charged SiO_2 sites, which accelerates the reduction in overall zeta potential at higher pH values.

3.5. Deposition of Janus Particles on Surfaces

Areal mass density of Janus SiO_2 MPs and PLL-SiO_2 MPs deposited on silicon dioxide and aluminum oxide surfaces at different pH are shown in Figure 6. In these Figures, the time zero reflects the time that particle suspension arrived the QCM-D channel. Initially, the number of particles deposited onto the QCM-D sensor is smaller than the detection threshold; therefore, no deposition was detected. On silicon dioxide surface at pH 7, the attachment rate of Janus SiO_2 MPs (Figure 6A) was 2.5 ng/cm^2-min and the areal mass of Janus SiO_2 MPs reached 69.7 ng/cm^2 at the end of the experiment. PLL-SiO_2 MPs (Figure 6B) had a higher attachment rate and areal mass compared with Janus SiO_2 MPs, which are 7.7 ng/cm^2-min and 219.5 ng/cm^2, respectively. No deposition was observed when control SiO_2 MPs flew on top of the silica oxide surfaces.

On aluminum oxide-coated surfaces at pH 7, control SiO_2 MPs (Figure 6C) deposited with attachment rate of 9.4 ng/cm^2-min. At the end of the experiment, the areal mass was 219.5 ng/cm^2. No deposition was observed when PLL-SiO_2 MPs nor Janus SiO_2 MPs flew on tope of the aluminum oxide-coated surfaces.

At pH 3, Janus SiO_2 MPs did not deposit onto aluminum oxide surfaces but deposited onto silicon dioxide surfaces, a similar trend at pH 7. The deposition of Janus SiO_2 MPs on silicon dioxide surface at pH 3 (Figure 6D) had an attachment rate of 2 ng/cm^2-min and at the areal mass reached 69.2 ng/cm^2. At pH 9, no deposition of Janus SiO_2 MPs occurred on silicon dioxide surfaces or on aluminum oxide surfaces at pH 9.

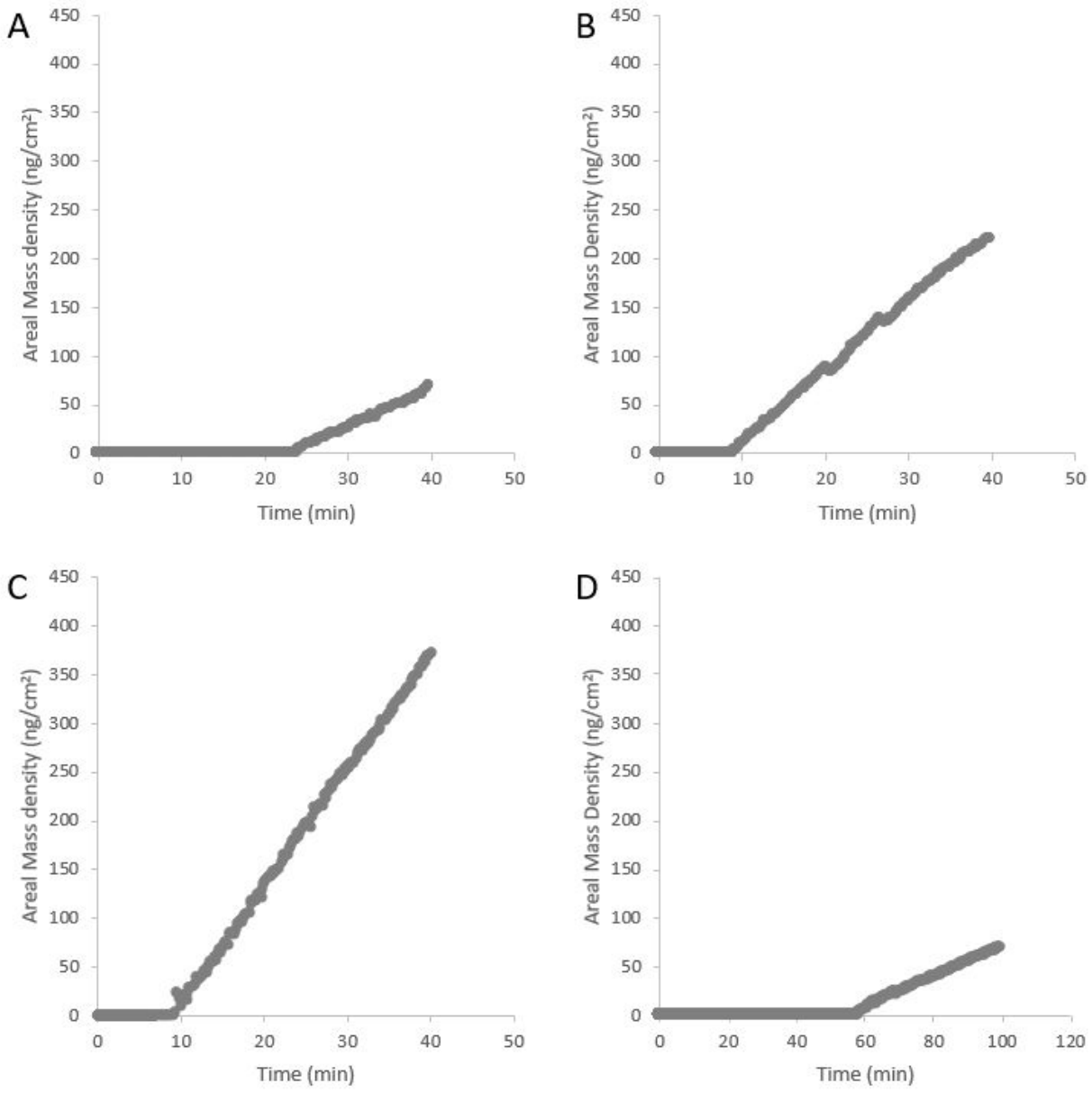

Figure 6. QCM-D deposition of (A) Janus SiO_2 MPs on silicon dioxide, (B) PLL-SiO_2MPs on silicon dioxide, (C) control SiO_2 MPs on alumina in 1 mM NaCl pH 7, and (D) Janus SiO_2 MPs on silicon dioxide at pH 3.

3.5.1 Deposition onto silicon dioxide surfaces

For control SiO_2 MPs, no deposition was observed from the QCM-D experiments when flowing on top of the silicon dioxide surfaces. This result was expected because the control SiO_2

MPs and silicon dioxide surfaces are both negatively charged. According to the DLVO theory, no deposition is expected under such unfavorable conditions. The deposition of Janus SiO_2 MPs (Figure 6A) on silicon dioxide surfaces was not detectable until about 24 minutes, while the deposition of PLL-SiO_2 MPs (Figure 6B) on silicon dioxide surfaces was detectable at about 9 minutes. This can be attributed to the smaller attachment rate of Janus SiO_2 MPs than PLL-SiO_2 MPs. Smaller attachment rate will require longer time to accumulate enough mass to reach the detection threshold of the instrument. Also due to the smaller attachment rate, less Janus SiO_2 MPs mass was attached after 40 minutes of experiments than PLL-SiO_2 MPs.

The smaller attachment rate of Janus SiO_2 MPs onto silicon dioxide surfaces can be attributed to presence of PLL on the surface, or the surface heterogeneity impact. While PLL-SiO_2 MPs were positively charged and attractive to silicon dioxide surfaces, only part of the Janus SiO_2 MPs surfaces was covered with positively charged PLL. We speculated that Janus SiO_2 MPs were not immediately captured when they approach the silicon dioxide surface. Particles close to the surface flow along the surface for some time until they diffuse away or are captured. During this movement, the surface of Janus SiO_2 MPs was sampled by the silicon dioxide surface. While particles have both rotational and translational movement, deposition occurs only when a sufficiently large area of PLL-covered surface faces the silicon dioxide surface. Previous experimental and modeling work [18,19] demonstrated that the attachment of heterogeneously charged particles is dependent on the possibility of heterogeneous patches facing the collector surface when particles rotate. Therefore, deposition of Janus SiO_2 MPs onto the silicon dioxide surfaces began to occur later and slower than the deposition of PLL-SiO_2 MPs, whose particle surfaces were homogeneously coated with positively charged PLL.

3.5.2 Deposition onto aluminum oxide surfaces

In QCM-D experiments for aluminum oxide-coated surfaces, attachment occurred only for control SiO_2 MPs (Figure 6C). The control SiO_2 MPs in the solution were negatively charged. A positive charge of 25 mV was reported for a thin ALD layer of alumina on the surface of a silica wafer at pH 7 in 1 mM KCl, [310] which was close to the conditions here. Assuming that the alumina-coated QCM-D sensor was also positively charged here, electrostatic attraction between control SiO_2 MPs and the alumina-coated QCM-D sensor is expected based on DLVO theory, which explains the observed deposition. As expected, no deposition occurred when the PLL-SiO_2 MP suspension flowed onto the aluminum oxide surface because both the PLL-SiO_2 MPs and aluminum oxide surface were positively charged.

However, no deposition was observed for Janus SiO_2 MPs onto the aluminum oxide surface. Janus SiO_2 MPs were partially negatively charged and partially positively charged, with an overall zeta potential of approximately 1.7 mV (Figure 5). The aluminum oxide surface and the negative part of the Janus particle surface are attractive to each other, which should have resulted in deposition/attachment of Janus SiO_2 MPs on the surface to some extent. We suspect that PLL played an important role in the interaction between Janus SiO_2 MPs and the aluminum oxide surface. Previous work [276,321] has indicated that PLL is mainly in a random coil formation at neutral pH. A random coil is a relatively loose structure, which can be as long as 200 nm at pH 7. [3029] We postulate that when Janus SiO_2 MPs approached the aluminum oxide surface, the stretched random-coiled PLL chains may form repulsive interactions with the aluminum oxide surface from a relatively far distance, which may prevent Janus SiO_2 MPs from further approaching the surface and inhibit deposition.

3.5.3 Role of pH on Janus SiO_2 NP deposition

In the previous sections, we observed that at pH 7, Janus SiO_2 MPs did not deposit onto aluminum oxide surfaces but deposited onto silicon dioxide surfaces. At pH 3, similar trend was observed for Janus SiO_2 MPs. However, no deposition occurred on silicon dioxide surfaces or on aluminum oxide surfaces at pH 9. The overall zeta potential of Janus SiO_2 MPs was negative at pH 9 (figure 5). According to DLVO theory, we would expect deposition of Janus SiO_2 MP on aluminum oxide surfaces. In summary, under all pH conditions, Janus SiO_2 MPs did not attach onto positively charged aluminum oxide surfaces, which indicates possibly a very critical role of surface heterogeneity, or the presence of positively charged PLL on the deposition.

Kataoka et al. [332] found that PLL adopted a random coil conformation at pH values lower than 4.3 and an α-helix conformation for pH values higher than 10. A mixture of random coil and α-helix structures is present between these pH values. The decrease in pH induced an increase in the positive charge density, which resulted in uncoiling of the PLL structure and increased the affinity of PLL to water. [343,354] The swollen PLL chains at pH 3 carried a positive charge, which created an electrostatic attraction with negatively charged silicon dioxide surfaces, leading to some attachment (Figure 6D). However, the electrostatic repulsion between the swollen PLL chains and aluminum oxide surfaces prevents deposition onto aluminum surfaces. At a low pH value, the PLL chain was about 200 nm long. [366] Therefore, when Janus SiO2 MPs approach the positively charged the aluminum surface, the long PLL chain suppressed the possible attraction between the aluminum surface and the negatively charged portion of the Janus particle surface. With increasing pH, some α-helix structures began to form. At neutral pH, the PLL conformation was still largely a random coil, and thus, the deposition behavior of Janus SiO_2 MPs was similar at pH 3 and pH 7.

At pH 9, more PLL was in a α-helix conformation, which is a much-compressed formation. The length of PLL at pH 9 is about 100 nm, only half of the length at lower pH values. Therefore, a lot of negatively charged sites on the surface of SiO_2 MPs were exposed. Also, previous work has found that the charge on the surface of PLL decreased with increasing pH. [35] Therefore, the part of Janus SiO_2 MP surface covered with PLL has weakly positively charged PLL and negatively charged Janus SiO_2 MPs sites simultaneously exposed to the surfaces. This highly heterogeneous charge distribution may result in complicated attraction and repulsion between Janus SiO_2 MPs and both the aluminum oxide and silicon dioxide surfaces, so that Janus SiO_2 MPs do not have the opportunity to access the adjacent surfaces; therefore, no deposition occurs. In order to rigorously verify the proposed role of PLL on Janus SiO2 MP deposition under various pH conditions, additional systematic study at the micromolecular level, on the conformation and charge distribution of PLL on the surface of Janus SiO_2 MPs, is needed, which is out of the scope of this study.

4. Conclusion

In this work, we have engineered Janus SiO_2 MPs, negatively charged SiO_2 MPs partially covered with positively charged PLL, as model particles to study the impact of particle surface heterogeneity on the deposition. Our work highlighted the important role of particle surface heterogeneity in the deposition of nanoparticles. This work found that the deposition of particles is more sensitive to particle surface heterogeneity properties than to the overall surface potential of the particles. For some situations in our experiments, deposition did not occur even though the overall zeta potential of Janus SiO_2 MPs was opposite that of the deposition surface, and this result was due to the dominant role of particle surface heterogeneity created by PLL. In such

conditions, an overall surface zeta potential will not be able to predict the interactions between nanoparticles and surfaces.

In the natural environment, the surfaces of particles are always heterogeneously charged and may partially be covered with natural organic matter or other functional groups. The particle surface heterogeneity properties may play a more important role in deposition than the overall surface potential of particles. To better predict their transport, nanoparticles must be better characterized, and the role of particle surface heterogeneity should be incorporated into modeling. The results of this study will provide guidance on modeling the transport and deposition of nanoparticles with heterogeneously charged surfaces in environmental settings.

Acknowledgments

This work is supported by National Science Foundation under grants EAR-1521428, CBET-1511941 and CBET- 1836799, and by ACS Petroleum Research Fund # 59374. The research was performed in part in the Nebraska Nanoscale Facility: National Nanotechnology Coordinated Infrastructure and the Nebraska Center for Materials and Nanoscience, which are supported by the National Science Foundation under Award ECCS: 1542182, and the Nebraska Research Initiative. Particularly, we would like to thank Dr. Lanping Yue on assisting the KPFM imaging.

Conflicts of interest

Authors declare no conflict of interest.

References

1. Yao KM, Habibian MT, O'Melia CR. Water and waste water filtration. Concepts and applications. Environmental science & technology. 1971 Nov 1;5(11):1105-12.

2. VanNess K, Rasmuson A, Ron CA, Johnson WP. A unified force and torque balance for colloid transport: Predicting attachment and mobilization under favorable and unfavorable conditions. Langmuir. 2019 Jun 10;35(27):9061-70.

3. Molnar IL, Johnson WP, Gerhard JI, Willson CS, O'carroll DM. Predicting colloid transport through saturated porous media: A critical review. Water Resources Research. 2015 Sep;51(9):6804-45.

4. Elimelech M, Nagai M, Ko CH, Ryan JN. Relative insignificance of mineral grain zeta potential to colloid transport in geochemically heterogeneous porous media. Environmental science & technology. 2000 Jun 1;34(11):2143-8.

5. Ron CA, VanNess K, Rasmuson A, Johnson WP. How nanoscale surface heterogeneity impacts transport of nano-to micro-particles on surfaces under unfavorable attachment conditions. Environmental Science: Nano. 2019;6(6):1921-31.

6. Salerno MB, Flamm M, Logan BE, Velegol D. Transport of rodlike colloids through packed beds. Environmental science & technology. 2006 Oct 15;40(20):6336-40.

7. Liu Q, Lazouskaya V, He Q, Jin Y. Effect of particle shape on colloid retention and release in saturated porous media. Journal of environmental quality. 2010 Mar;39(2):500-8.

8. Wang P, Keller AA. Natural and engineered nano and colloidal transport: Role of zeta potential in prediction of particle deposition. Langmuir. 2009 Jun 16;25(12):6856-62.

9. Drelich J, Wang YU. Charge heterogeneity of surfaces: Mapping and effects on surface forces. Advances in colloid and interface science. 2011 Jul 11;165(2):91-101.

10. Seymour MB, Chen G, Su C, Li Y. Transport and retention of colloids in porous media: does shape really matter?. Environmental science & technology. 2013 Aug 6;47(15):8391-8.

11. Aramrak S, Flury M, Harsh JB, Zollars RL, Davis HP. Does colloid shape affect detachment of colloids by a moving air–water interface?. Langmuir. 2013 May 14;29(19):5770-80.

12. Xu S, Liao Q, Saiers JE. Straining of nonspherical colloids in saturated porous media. Environmental science & technology. 2008 Feb 1;42(3):771-8.

13. Barua S, Yoo JW, Kolhar P, Wakankar A, Gokarn YR, Mitragotri S. Particle shape enhances specificity of antibody-displaying nanoparticles. Proceedings of the National Academy of Sciences. 2013 Feb 26;110(9):3270-5.

14. Pazmino E, Trauscht J, Johnson WP. Release of colloids from primary minimum contact under unfavorable conditions by perturbations in ionic strength and flow rate. Environmental science & technology. 2014 Aug 19;48(16):9227-35.

15. Liu J, Gaikwad R, Hande A, Das S, Thundat T. Mapping and quantifying surface charges on clay nanoparticles. Langmuir. 2015 Sep 29;31(38):10469-76.

16. Baitimirova M, Osite A, Katkevich J, Viksna A. Electrochemical Characteristics of Particulate Matter. Rigas Tehniskas Universitates Zinatniskie Raksti. 2011 Jul 1;7:19.

17. Shave MK, Kalasin S, Ying E, Santore MM. Nanoscale functionalized particles with rotation-controlled capture in shear flow. ACS applied materials & interfaces. 2018 Aug 15;10(34):29058-68.

18. Li K, Ma H. Rotation and retention dynamics of rod-shaped colloids with surface charge heterogeneity in sphere-in-cell porous media model. Langmuir. 2019 Mar 29;35(16):5471-83.

19. Ron CA, Johnson WP. Complementary colloid and collector nanoscale heterogeneity explains microparticle retention under unfavorable conditions. Environmental Science: Nano. 2020;7(12):4010-21.

20. Chen Q, Diesel E, Whitmer JK, Bae SC, Luijten E, Granick S. Triblock colloids for directed self-assembly. Journal of the American Chemical Society. 2011 May 25;133(20):7725-7.

21. Chen Q, Yan J, Zhang J, Bae SC, Granick S. Janus and multiblock colloidal particles. Langmuir. 2012 Sep 25;28(38):13555-61.

22. Jiang S, Chen Q, Tripathy M, Luijten E, Schweizer KS, Granick S. Janus particle synthesis and assembly. Advanced materials. 2010 Mar 12;22(10):1060-71.

23. Ling XY, Phang IY, Acikgoz C, Yilmaz MD, Hempenius MA, Vancso GJ, Huskens J. Janus particles with controllable patchiness and their chemical functionalization and supramolecular assembly. Angewandte Chemie International Edition. 2009 Sep 28;48(41):7677-82.

24. Shinde SS, Park S, Shin J. Spin synthesis of monolayer of SiO 2 thin films. Journal of Semiconductors. 2015 Jan 25;36(4):043002-10.

25. Liu J, Gaikwad R, Hande A, Das S, Thundat T. Mapping and quantifying surface charges on clay nanoparticles. Langmuir. 2015 Sep 29;31(38):10469-76.

26. Wang Y, Chang YC. Synthesis and conformational transition of surface-tethered polypeptide: poly (L-lysine). Macromolecules. 2003 Aug 26;36(17):6511-8.

27. Hong L, Cacciuto A, Luijten E, Granick S. Clusters of charged Janus spheres. Nano letters. 2006 Nov 8;6(11):2510-4.

28. Metin CO, Lake LW, Miranda CR, Nguyen QP. Stability of aqueous silica nanoparticle dispersions. Journal of Nanoparticle Research. 2011 Feb;13(2):839-50.

29. Naassaoui I, Aschi A. Evaluation of properties and structural transitions of Poly-L-lysine: effects of pH and temperature. Journal of Macromolecular Science, Part B. 2019 Aug 3;58(8):673-88.

30. Gu D, Yalcin S, Baumgart H, Qian S, Baysal O, Beskok A. Electrophoretic light scattering for surface zeta potential measurement of ALD metal oxide films. ECS Transactions. 2010 Oct 1;33(2):37.

31. Chen KL, Elimelech M. Aggregation and deposition kinetics of fullerene (C60) nanoparticles. Langmuir. 2006 Dec 19;22(26):10994-1001.

32. Kataoka K, Ishihara A, Harada A, Miyazaki H. Effect of the Secondary Structure of Poly (l-lysine) Segments on the Micellization in Aqueous Milieu of Poly (ethylene glycol)− Poly (l-lysine) Block Copolymer Partially Substituted with a Hydrocinnamoyl Group at the Nε-Position. Macromolecules. 1998 Sep 8;31(18):6071-6.

33. Bordi F, Cametti C, Paradossi G. High-frequency dielectric study of side-chain dynamics in poly (lysine) aqueous solutions. Biopolymers: Original Research on Biomolecules. 2000 Feb;53(2):129-34.

34. Guo Y, Ma Y, Xu L, Li J, Yang W. Conformational change induced reversible assembly/disassembly of poly-L-lysine-functionalized gold nanoparticles. The Journal of Physical Chemistry C. 2007 Jul 5;111(26):9172-6.

35. Lee S, Spencer ND. Adsorption properties of poly (L-lysine)-graft-poly (ethylene glycol)(PLL-g-PEG) at a hydrophobic interface: Influence of tribological stress, pH, salt concentration, and polymer molecular weight. Langmuir. 2008 Sep 2;24(17):9479-88.